Silica-based diffusion probes for use in FRAP and NMR-diffusometry

Citation for the original published paper (version of record):
Pihl, M., Kolman, K., Lotsari, A. et al (2019). Silica-based diffusion probes for use in FRAP and NMR-diffusometry. Journal of Dispersion Science and Technology, 40(4): 555-562.
http://dx.doi.org/10.1080/01932691.2018.1472015

In the FRAP technique, the fluorescence of a probe is deactivated by fast laser beam irradiation. The recovery of the fluorescence of the bleached area, resulting from the diffusion-in of the non-bleached diffusion probe and the diffusion-out of the deactivated probe, is monitored as function of time. When the probe diffuses freely in the sample, that is without interaction with the structure of the soft matrix, the recovery curves allows the determination of the diffusion coefficient and by use of the Stokes-Einstein relationship, the probe size.[13] Because of the principle of measurement, the probe has of course to bear a chromophore which fluorescence can be annihilated by a laser intensity that does not alter the material structure. Furthermore the material studied must present a certain transparency at the laser wavelength to allow the laser beam penetration. One important feature of FRAP is the fact that it allows local diffusion measurements at the micrometer scale, thus introducing spatial resolution in the nature of the measurements.

NMR-d provides a macroscopic evaluation of the diffusion, due to the fact that the measurement is applied to the whole material, thus often yielding an average diffusion value.[18] Diffusion measurements by NMR are based on the well-established spin-echo sequence in presence of vertical gradients of varying strength and is most often done by monitoring proton rich species response with ^{1}H NMR. In that case, water or pegylated molecules are often used as a probe.

Even though NMR-d and FRAP measure diffusion in heterogeneous materials, these techniques differ on several points. NMR-d measures global diffusion of the probe, over a large domain, whereas FRAP provides a local measurement, from the bleached region. NMR-d acquisition time is usually dependent on the probe concentration, which is higher than for FRAP, especially to manage short measurement times. FRAP is more sensitive, facilitating lower probe concentrations. By using both methods, it is possible to compare global and local diffusion to gain knowledge on the heterogeneity of the material and on probe-material interactions.[18] However, the direct comparison of the results obtained on a given system by both techniques is often very difficult, mainly because of the use of two different probes. Two probes are necessary as there is a lack of available material showing the requested features, namely fluorescence and presence of NMR-responsive protons. Silica nanoparticles lend themselves very well for this purpose, in the sense that their little size and high specific surface provides a versatile platform to introduce both fluorescence and a good NMR response as they can be derivatized by oligomeric species such as polyethylene glycol, which are usually easy to identify by ^{1}H NMR. In addition, it is also possible to control the size of silica particles from a few nanometer up to hundreds.

In this study, we have synthesized and modified silica nanoparticles detectable by FRAP and NMR-d to be used as probes for measuring diffusion. Fluorescence was obtained using fluorescein isothiocyanate (FITC) or Rhodamine B isothiocyanate (RITC) precursors, whereas polyethyleneglycol (PEG) provided a NMR-d responsive moiety. Diffusion constants in water were measured and showed good agreement between the two techniques, indicating the potential of using modified silica nanoparticles for diffusion measurements.

Materials and methods

Materials

Ammonia solution 25% (Merck Millipore), tetraethyl orthosilicate (TEOS, Sigma-Aldrich), ethanol 99.5% (Solveco), (3-aminopropyl)trimethoxysilane (APTMS, Sigma-Aldrich), fluorescein isothiocyanate isomer I (FITC, Sigma-Aldrich), Rhodamine B isothiocyanate (RITC, Sigma-Aldrich) and 2-[methoxy(polyethyleneoxy)propyl]trimethoxysilane ($n = 21$–24 EO units, Gelest) were used without further purification. MilliQ water (resistivity >18 M Ω) was used for preparation of the aqueous solutions.

Fluorescent silica particle synthesis

The silica particle production was based on the Stöber process adapted and reported by Zhang et al.[19] and Estevéz et al.[20] All glassware were filled with water and sonicated for 15 minutes before use. A fluorescent conjugate was prepared by mixing FITC or RITC and (3-aminopropyl)trimethoxysilane, APTMS, in ethanol and stirring for 24 hours. Concentrations are reported in Table 1. The conjugate was then mixed with ammonia, water and ethanol before a dropwise addition of TEOS was carried out, and stirred for another 24 hours (Table 1). To increase particle and photostability, and obtain smooth nanoparticles, a TEOS coating was performed by a further addition of TEOS and stirring for 24 hours. For one sample, FluoSil5, a second TEOS layer was added. The samples were purified by centrifugation (15 minutes, 2500 rpm, ALC 4233 ECT centrifuge) and subsequent ultrafiltration using a 30 kDa cut-off ultrafiltration disc (Amicon Merck Millipore). The samples were tested for free FITC with a spectrofluorometer (Shimadzu RF-5000 DR-15) at 494 nm.

Pegylation of the silica particles

The silica particles were PEG modified using 2-[methoxy(-polyethyleneoxy)propyl]trimethoxysilane. The specific surface area, S in m^2/g, was calculated using radii r obtained from TEM measurements, a density ρ of 2.6 g/cm^3 was used in the following equation, as for plain silica.

$$S = \frac{3}{\rho r} \quad [1]$$

Using the measured weight percent of silica and the maximum known number of 8 $\mu mol/m^2$ of surface silanol groups, the total number of silanol groups were calculated and subsequently used to determine the amount of PEG silane needed to surface modify all the available silanol groups, allowing the reaction to be carried out in excess of PEG silane modifier. Approximately 1 ml of PEG was prepared in MilliQ water adjusted to pH 10. Silica particles (0.37–1 wt%) were added to a round flask and heated to 80 °C, after which the PEG was added at an addition rate of

Table 1. Concentration of chemicals to produce fluorescent silica particles.

Samples	TEOS [M]	TEOS coat [mM]	2nd TEOS coat [mM]	NH_3 [M]	H_2O [M]	FITC [mM]	RITC [mM]	APTMS [mM]
FluoSil1	0.167	–	–	0.557	1.58	0.190	–	0.992
FluoSil2	0.167	29.4	–	0.557	1.58	0.190	–	0.992
FluoSil3	0.167	29.4	–	0.557	1.58	0.364	–	0.722
FluoSil4	0.167	29.4	–	0.557	1.58	0.348	–	1.44
FluoSil5	0.166	29.2	29.2	0.553	1.57	0.370	–	1.43
FluoSil6	0.33	–	–	0.550	1.55	0.160	–	1.47
FluoSil7	0.33	–	–	0.550	1.55	–	0.160	1.47
FluoSil8	0.22	3.83		0.579	1.64	0.372		1.50

2 μmol·m^{-2}·h^{-1}. using a NE-1000 Programmable Single Syringe Pump (New Era Pump Systems Inc.). The reaction was then allowed to continue for another 2 hours before purification as described above. Samples prepared that way are reported as FluoSil#PEG, # being a numerical.

Transmission electron microscopy, TEM

A JEOL JEM-1200 EX II electron microscope operated at 120 kV and a FEI Tecnai G2 T20 electron microscope operated at 200 kV were used to visualize particles and take images. Microscopy specimens were prepared by submerging a holey carbon coated copper grid for 1 minute in 0.1 wt% silica particle dispersion and then air drying. More than 200 particles were used in order to obtain statistically relevant size distributions with the software ImageJ.

Dynamic light scattering, DLS

A N4 Plus submicron particle analyser (Beckman Coulter) was used for DLS measurements. The dispersions were diluted to a concentration of 0.05 wt% and filtered through 0.8 μm hydrophilic syringe filter. The measurements were performed at a scattering angle of 90° for 5 minutes. The obtained autocorrelation functions were analysed using the CONTIN fitting routine,[21,22] which yielded a size distribution function. The fitting procedure was performed using Matlab R2014b.[23]

Fluorescence recovery after photobleaching, FRAP

A Leica SP2 AOBS (Heidelberg, Germany) confocal laser scanning microscope equipped with a 20×, 0.5 NA water objective was used for FRAP measurements. The settings used were 256 × 256 pixels, zoom factor 4 (with a zoom-in during bleaching), and 800 Hz, yielding a pixel size of 0.73 μm and an image acquisition rate of two images per second. The FRAP images were stored as 12-bit tif-images. The 488 nm line of an argon laser was utilized to excite the fluorescent probes. The beam expander was set to 1, which lowered the effective NA to approximately 0.35 and yielded a slightly better bleaching and a more cylindrical bleaching profile. The bleached areas, region of interest (ROI), were 30 μm large discs (nominal radius rn =15 μm) 50 μm into the sample. The measurement routine consisted of 20 prebleach images, 1 bleach image - gaining an initial bleaching depth ≈ 35% of the prebleach intensity in the ROI - and 50 postbleach frames, recording the recovery. The FRAP data were normalized by the prebleach fluorescence intensity and analysed with a pixel-based model.[24]

Seven microliters of probe solutions, diluted in neutral water about 500 times, were placed into secure-seal spacer grids (120 μm thick, 9 mm diameter, Invitrogen, USA) between two cover glass slides. FRAP measurements were carried out in room temperature on a dilution series of the probe, until the fluorescent signal was too weak to yield accurate measurements.

Nuclear magnetic resonance diffusometry, NMR-d

Diffusion experiments were run on a 14.1 T Bruker spectrometer (600 MHz) equipped with a Diff30 probe at 22 °C. 1H diffusion measurements were carried out in the z-direction by using a standard two pulse stimulated echo sequence. The gradient strength, G, was varied linearly in at least 16 steps, between 90 and 750 Gauss/cm. The gradient duration δ was set to 1 ms and the time between the leading edges of the two gradient pulses that allow for diffusive motion Δ was set to 100 ms. For each sample, 256 scans were collected using the parameters determined for a 90° pulse (P1 ∼ 11μs, D1 = 8s). The processing (phasing, baseline correction, integration and diffusion constant determination) was done with TopSpin (Bruker, Germany). Measurements were performed on nanoparticles in their storage solution, water at pH 10.

Results and discussion

Silica nanoparticle synthesis and characterisation

Silica nanoparticle probes measurable by both FRAP and NMR-d technique were prepared. As is shown in Figure 1, the organic fluorophores FITC or RITC, probed in FRAP, are incorporated into silica nanoparticle cores by forming a dialkyl thiourea with aminopropyltrimethoxy silane. This preconjugate is then incorporated in a silica matrix formed during the hydrolysis and condensation of TEOS in a mixture of water, ethanol and ammonia,[25] thus forming fluorescent colloidal silica. Trapping of fluorophore inside the particle also has the benefit of reduced dye leakage. Low concentrations of TEOS were used (0.167–0.33 M) in order to reduce the risk of aggregation.[26] Despite variations in concentration of TEOS, FITC and APTMS, all the synthesis resulted in particles with the main fraction having size around 40 nm (Table 2 and Figure 3). This procedure yielded particles onto which a further TEOS layer was

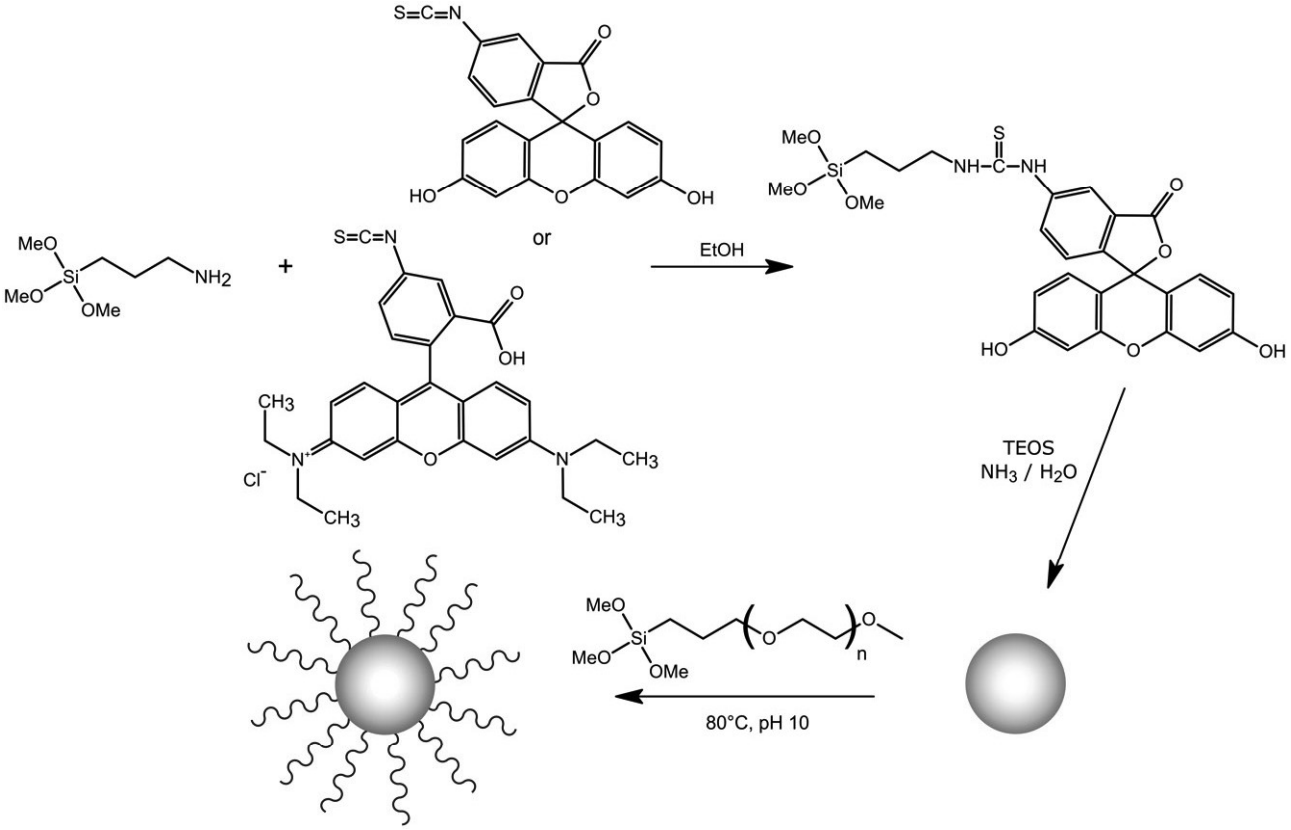

Figure 1. Synthesis of fluorescent and PEG functionalized silica particles.

Table 2. Particle characterisation.

Sample	Diameter TEM [nm]	Diameter DLS [nm]	Diameter FRAP [nm]	Diameter NMR-d [nm]
FluoSil 1			40–46	
FluoSil 2			40–46	
FluoSil 3				
FluoSil 3-PEG	41 ± 6		34 ± 1	
FluoSil 4				
FluoSil 4-PEG	38 ± 8			34 ± 2
FluoSil 5			41 ± 3	
FluoSil 5-PEG	37 ± 5		49 ± 2	48 ± 3
FluoSil 6	42 ± 4	20–50		
FluoSil 7		20–90		
FluoSil 8-PEG	32 ± 7			40 ± 2

applied. Such an extra coating is known to be beneficial when it comes to increasing the photostability,[27,28] obtaining a smoother surface[19] and providing a pure silica surface that may be further modified.[29] In the present case, the second coating also made the particle suspensions appear more homogenous, that is less aggregated, which seemed to imply that an additional silica layer rendered the particles more stable.

The ^{1}H NMR responsive moiety was introduced via surface modification of the fluorescent silica particles by PEG-silane. The reaction was carried out under alkaline conditions in order to promote the methoxy silylether hydrolysis, and the rate of addition was controlled to limit the derivatizing agent self-condensation. Purification was carried out by ultrafiltration. Pegylation of the surface enhanced the water dispersibility. It is also know to reduce the interaction with, for instance, biomolecules.[30] In the present case, such feature is also beneficial in the sense that it reduces the risk of having the diffusion probe interacting with the material studied.

Figure 2 shows the Bright Field (BF) TEM micrographs of the resulting particles. The core-shell structure of the particles can be clearly seen. All obtained particles, despite the second layer of TEOS added to obtain smoother particles, had a faceted structure. In general, smaller particles produced by the Stöber process are less smooth and spherical and have higher surface roughness.[31] Figure 2c shows degradation of the fluorescent core due to extended exposure of the particles to the electron beam of TEM. The TEM measurements revealed also that the pegylation did not affect the particle structure significantly. The particle sizes were determined by DLS and from TEM images and varied from 20–90 nm in diameter (Table 2 and Figure 3).

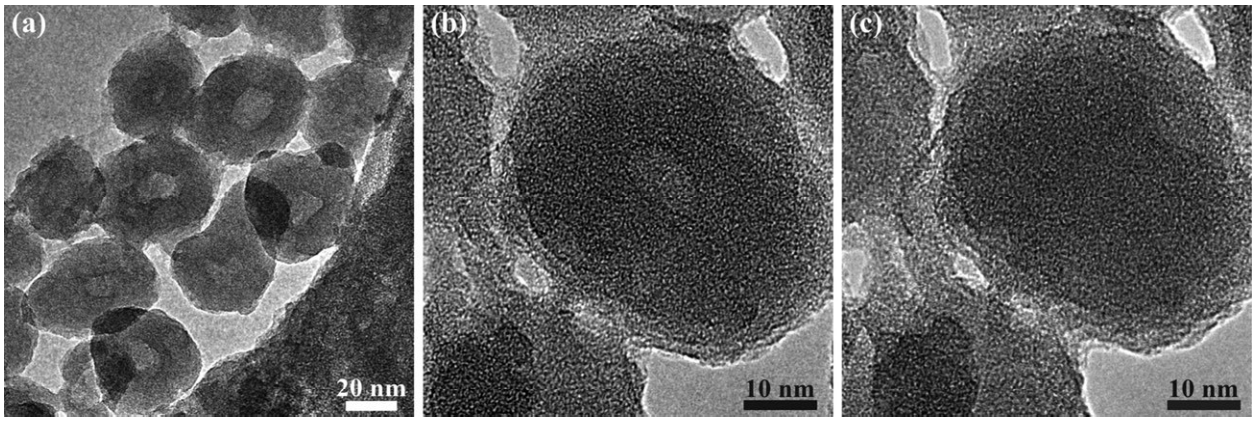

Figure 2. BF TEM images showing the core-shell structure of silica particles FluoSil6 (a, b) at different magnifications. Longer exposure of the particles to electron beam caused degradation of the fluorescent core (c).

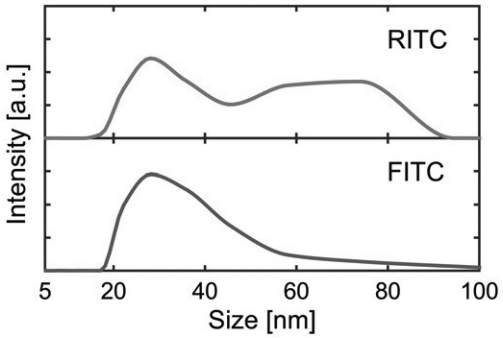

Figure 3. Size distributions of FluoSil6 (FITC) and FluoSil7 (RITC) obtained by DLS.

FRAP measurements

Prior to the diffusion measurements, the bleachability of the particle was evaluated.[25] Probes used for FRAP should have intermediate photostability, allowing both bleaching of the region of interest and imaging of the recovery process.[14] Dye-doped silica nanoparticles have the benefits of high fluorescent intensity, good photostability, stability in aqueous environment, ease of manufacturing and a silica surface that is easily modified.[29]

The silica nanoparticles FluoSil2 showed good bleachability, that is the particles were bleachable even with the dye incorporated into the silica matrix. The coating of TEOS was added to increase the photostability of the dye-doped silica nanoparticles. However, this may also decrease the tendency of the particles for bleaching, which can be a drawback for FRAP measurements. The FRAP measurements showed the TEOS coat to be beneficial, with better stability and particles requiring a higher intensity laser pulse for bleaching compared to non-coated particles (FluoSil1). The level of fluorescence for FluoSil2 was reasonable for FRAP experiments but the FITC concentration was almost doubled for subsequent particle batches to increase the fluorescence signal intensity (FluoSil3 and FluoSil4). However, there is a limit to how high an intensity that can be obtained as when dye molecules come too close together the molecules go from their excited state without emitting a photon,[25] that is self-quenching. Because of this the dye concentrations should be kept low. The maximum concentration of the fluorescent stain Rubpy incorporated into silica nanoparticle matrix which can be used before self-quenching occurs, is 0.7 mM.[29] When surface-attaching FITC, van Blaaderen et al. used FITC concentrations in the range of 0.45–5.6 mM for 240–1000 nm particles[25] to avoid self-quenching. Here 0.16–0.37 mM FITC and 0.16 mM RITC were used to incorporate the dye-conjugate inside 40 nm particles.

As the reaction between FITC and APTMS is usually incomplete, non-reacted FITC remains in solution and is thus not incorporated in the silica matrix. The effect of APTMS concentration in the FITC preconjugate formation was therefore investigated to evaluate if a higher APTMS concentration could improve the yield of the conjugate formation while keeping the Stöber process not affected. FRAP measurements were carried for samples FluoSil3 and FluoSil5 and showed better results for the latter, that is the higher APTMS concentrations, which was used for subsequent surface modification.

Surprisingly, the pegylated particles demanded a higher laser intensity to be bleached compared to the non-pegylated ones. A tentative explanation can be that the protection of the dye results from the surface light scattering due to the grafted PEG. No investigation of this phenomena was carried out, however.

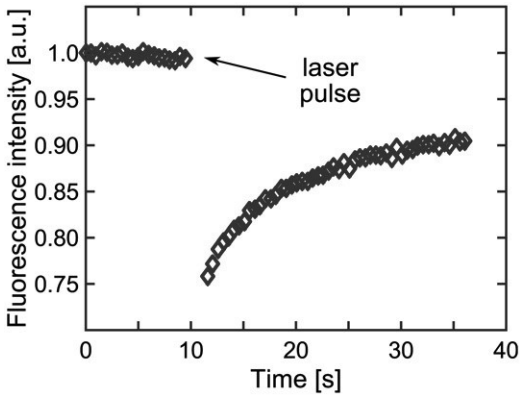

Figure 4. Fluorescence intensity recovery profile for FluoSil5PEG at room temperature.

Table 3. Self-diffusion coefficients for dye-doped silica nanoparticles, calculated from FRAP and NMR-d measurements.

Sample	Self-diffusion coefficient FRAP [$\mu m^2/s$]	Self-diffusion coefficient NMR-d [$\mu m^2/s$]
FluoSil 3-PEG	10.55	
FluoSil4 -PEG		13.33
FluoSil 5	12.90	
FluoSil 5-PEG	8.78	9.48
FluoSil 8-PEG		11.30

Figure 4 shows a typical FRAP curve, where one can see the bleaching effect of the laser pulse on the intensity at 10 seconds, followed by the fluorescence recovery as a result of the diffusion of the fluorescent probe in the bleached region while extinguished species diffuse out.

For FRAP measurements the particles are relatively large, making the diffusion, and consequently the recovery, slow. Because of this, only enough of the recovery was recorded to make an accurate analysis, see Figure 4. The lowest probe concentration yielding accurate and reliable FRAP results was 450 ppm. The self-diffusion constants were determined to 8.8–12.9 $\mu m^2/s$ and the particle sizes were determined to 33–49 nm in diameter in the FRAP measurements (Tables 2–3), using the Stokes-Einstein law, see Equation (2).

$$D = \frac{K_B T}{6\pi\eta R} \quad [2]$$

where D is the diffusion coefficient, k_B is Boltzmann's constant, T is the absolute temperature and η is the viscosity of the medium. R is the hydrodynamic radius of the particle. In the present case, viscosity of water at 25 °C was used (0.89 mPa × s).

The sizes determined were slightly higher that that determined by TEM. In TEM however, particles often shrink when exposed to vacuum and the beam. Furthermore, in FRAP, the hydrodynamic radius is measured whereas in TEM the silica particle core is measured, which might also slightly influence the results.

NMR diffusometry measurements

The pegylated silica particles showed good ^1H NMR signal (see Figure S1, supporting information) and their diffusion coefficient was therefore determined using a pulsed field gradient NMR sequence. The results were analysed using the Stejskal-Tanner equation[32]:

$$I = I_0 \exp\left\{-\frac{\Delta}{T_2}\right\} \exp\left\{(\gamma\delta G)^2\left(\Delta - \frac{\delta}{3}\right)\right\} \quad [3]$$

In Equation (3), the intensity of the signal, I, is function of the intensity without gradient, I_0, the duration of the two gradient pulses, δ, the time between pulses, Δ, and the strength of the z-gradient pulse, G. T2 is the spin-spin relaxation time constant and γ is the gyromagnetic ratio. In practice, the diffusion coefficient, D, is determined by plotting $\log(I/I_0)$ against k, where

$$k = (\gamma\delta G)^2\left(\Delta - \frac{\delta}{3}\right) \quad [4]$$

In a system containing a single diffusing specie, a linear relationship is obtained, and the diffusion coefficient can be determined from the slope, as shown in Figure 5.

Figure 5a, shows the typical decay of the log of normalized intensity as function of G^2 for a system composed of a single diffusing specie. The single decay confirms the absence of free residue unbound from the particle. Figure 5b is an example of $\log(I/I_0)$ versus G^2 in the case of a two-component system, that is free PEG and the surface modified dye-doped silica nanoparticles, FluoSil5PEG. Two decays can be observed. The first decay reflect the fast diffusing component while the second decay results from the signal recovery of the slower diffusing specie. The capacity in discriminating different diffusing species is an important feature of NMR-d, distinguishing it from FRAP. FRAP cannot capture separately the diffusion of several diffusing substances in the sample, thus giving a mean diffusion value for all diffusing substances. Since smaller particles/molecules diffuse faster than larger ones, they will contribute unevenly to the overall diffusion coefficient. With NMR-d, such a biased diffusion constant can be avoided. The particles diameters measured in NMR-d varied between 34 and 48 nm and the self-diffusion constants were 9–13 $\mu m^2/s$ (Tables 2–3), which agreed reasonably well with the FRAP measurements.

Multi-purpose imaging probes have been developed as contrast agents to visualise tumours using MRI and optical

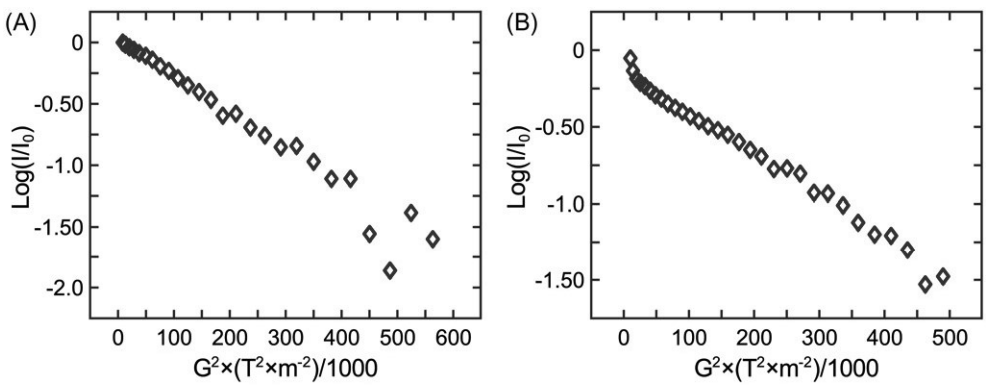

Figure 5. $Log(I/I_0)$ plotted versus $G^2 \times (T^2 \times m^{-2})$ for pure particles (a) and a two-component system of free PEG and PEG-modified dye-doped silica nanoparticles (b), as measured by NMR-d. The first points in the two-component system represent a faster diffusing component, the free PEG, while the diffusion of the silica particles is captured by the less steep slope (further details are given in Figures S2–S3).

techniques. Such probes include silica nanoparticles with a paramagnetic complex and a fluorescent moiety[33,34] as well as iron oxide nanoparticles conjugated with fluorochromes.[35] However, to our knowledge, multi-purpose probes to be used for diffusion studies using both FRAP and NMR-d have not been made. Direct comparisons between FRAP and NMR-d experiments often cannot be done as different probes are used[18] but here we show the possibility of using the same fluorescing, NMR-responsive probe in both techniques. The particles have fluorescence intensity and bleachability suitable for FRAP experiments and the pegylation provided a NMR-d responsive moiety.

As can be seen in Table 3, the self-diffusion coefficients are approximately the same, indicating the possibility of comparing the results between the techniques. The small differences may partly be explained by differences in pH during measurements, which would change the hydration of the non-modified silanol groups of silica particles.[36] Overall, it is a 7% difference which can be regarded as small. These results demonstrates that the probe can be used to measure variation in diffusion by two complementary techniques working at different lengthscale.

Conclusion

In this study we present the preparation of fluorescent, pegylated silica particles and how to utilise them as diffusional probes in FRAP and NMR-d. The size of the particles ranged from 20 nm to 90 nm, while the fluorescence of the silica nanoparticles enabled FRAP-response and pegylation allowed the detection of the particles by NMR.

The combination of these techniques provides information about both local and global diffusion, at different time and length scales and knowledge on mass transport, material heterogeneities and probe-material interactions can be obtained. The route chosen to prepare the probes, being based on silica condensation from TEOS, presents advantages and opens for a great versatility in terms of size and surface chemistry, and can be seen as a generic platform for further development of such type of probes. These results provide a range of synthesis conditions to prepare FRAP and NMR-responsive probe and give the parameter space to further adapt them to specific requirements.

Acknowledgments

The collaborations and financial support from SuMo Biomaterials is highly appreciated from all authors. The Swedish NMR Centre is acknowledged for spectrometer time.

Disclosure statement

No potential conflict of interest was reported by the authors.

Funding

Swedish Foundation for Strategic Environmental Research.

References

[1] Nydén, M.; Lorén, N.; Hermansson, A.-M. The Effect of Microstructure on Solvent and Solute Diffusion on the Micro- and Nanolength Scales. In *Water Properties of Food, Pharmaceutical, and Biological Materials*; Buera, M. d. P., Welti-Chanes, J., Lillford, P. J., Corti, H. R., Eds.; CRC Press: Boca Raton, **2006**; pp 79–100.

[2] Lorén, N.; Nydén, M.; Hermansson, A.-M. Determination of Local Diffusion Properties in Heterogeneous Biomaterials. *Adv. Colloid Interface Sci.* **2009**, *150*, 5–15. DOI:10.1016/j.cis.2009.05.004

[3] Brown, W. *Dynamic Light Scattering: The Method and Some Applications*; Clarendon Press: Oxford, **1993**.

[4] Berne, B. J.; Pecora, R. *Dynamic Light Scattering: With Applications to Chemistry, Biology, and Physics*; Courier Dover Publications: Mineola, **2000**.

[5] Levi, V.; Ruan, Q.; Gratton, E. 3-D Particle Tracking in a Two-Photon Microscope: Application to the Study of Molecular Dynamics in Cells. *Biophys. J.* **2005**, *88*, 2919–2928. DOI:10.1529/biophysj.104.044230

[6] Saxton, M. J. Single-Particle Tracking: The Distribution of Diffusion Coefficients. *Biophys. J.* **1997**, *72*, 1744–1753. DOI:10.1016/S0006-3495(97)78820-9

[7] Hess, S. T.; Huang, S.; Heikal, A. A.; Webb, W. W. Biological and Chemical Applications of Fluorescence Correlation Spectroscopy: A Review. *Biochemistry*. **2001**, *41*, 697–705.

[8] Oleg, K.; Grégoire, B. Fluorescence Correlation Spectroscopy: The Technique and Its Applications. *Rep. Prog. Phys.* **2002**, *65*, 251–297.

[9] Schuster, E.; Sott, K.; Strom, A.; Altskar, A.; Smisdom, N.; Geback, T.; Loren, N.; Hermansson, A.-M. Interplay Between Flow and Diffusion in Capillary Alginate Hydrogels. *Soft Matter*. **2016**, *12*, 3897–3907. DOI:10.1039/C6SM00294C

[10] Cheng, Y.; Prud'homme, R. K.; Thomas, J. L. Diffusion of Mesoscopic Probes in Aqueous Polymer Solutions Measured by Fluorescence Recovery After Photobleaching. *Macromolecules*. **2002**, *35*, 8111–8121. DOI:10.1021/ma0107758

[11] Hagman, J.; Lorén, N.; Hermansson, A.-M. Probe Diffusion in Î°-Carrageenan Gels Determined by Fluorescence Recovery After Photobleaching. *Food Hydrocolloids*. **2012**, *29*, 106–115. DOI:10.1016/j.foodhyd.2012.02.010

[12] Hagman, J.; Lorén, N.; Hermansson, A.-M. Effect of Gelatin Gelation Kinetics on Probe Diffusion Determined by FRAP and Rheology. *Biomacromolecules*. **2010**, *11*, 3359–3366. DOI:10.1021/bm1008487

[13] Deschout, H.; Hagman, J.; Fransson, S.; Jonasson, J.; Rudemo, M.; Loren, N.; Braeckmans, K. Straightforward FRAP for Quantitative Diffusion Measurements with a Laser Scanning Microscope. *Opt Express*. **2010**, *18*, 22886–22905. DOI:10.1364/OE.18.022886

[14] Lorén, N.; Hagman, J.; Jonasson, J. K.; Deschout, H.; Bernin, D.; Cella-Zanacchi, F.; Diaspro, A.; McNally, J. G.; Ameloot, M.; Smisdom, N.; et al. Fluorescence Recovery After Photobleaching in Material and Life Sciences: Putting Theory into Practice. *Q. Rev. Biophys.* **2015**, *48*, 323–387. DOI:10.1017/S0033583515000013

[15] Singer, J. R. NMR Diffusion and Flow Measurements and an Introduction to Spin Phase Graphing. *J. Phys. E: Sci. Instrum.* **1978**, *11*, 281–291. DOI:10.1088/0022-3735/11/4/001

[16] Price, W. S. Pulsed-Field Gradient Nuclear Magnetic Resonance as a Tool for Studying Translational Diffusion: Part 1. Basic Theory. *Concepts Magn. Reson.* **1997**, *9*, 299–336. DOI:10.1002/(SICI)1099-0534(1997)9:5<299::AID-CMR2>3.0.CO;2-U

[17] Bernin, D.; Topgaard, D. NMR Diffusion and Relaxation Correlation Methods: New Insights in Heterogeneous Materials. *Curr. Opin. Colloid Interface Sci.* **2013**, *18*, 166–172. DOI:10.1016/j.cocis.2013.03.007

[18] Wassen, S.; Bordes, R.; Geback, T.; Bernin, D.; Schuster, E.; Loren, N.; Hermansson, A.-M. Probe Diffusion in Phase-Separated Bicontinuous Biopolymer Gels. *Soft Matter*. **2014**, *10*, 8276–8287. DOI:10.1039/C4SM01513D

[19] Zhang, N.; Ding, E.; Feng, X.; Xu, Y.; Cai, H. Synthesis, Characterizations of Dye-Doped Silica Nanoparticles and Their Application in Labeling Cells. *Colloids Surf. B Biointerfaces*. **2012**, *89*, 133–138. DOI:10.1016/j.colsurfb.2011.09.017

[20] Estévez, M. C.; O'Donoghue, M.; Chen, X.; Tan, W. Highly Fluorescent Dye-Doped Silica Nanoparticles Increase Flow Cytometry Sensitivity for Cancer Cell Monitoring. *Nano Res*. **2009**, *2*, 448–461. DOI:10.1007/s12274-009-9041-8

[21] Provencher, S. W. CONTIN: A General Purpose Constrained Regularization Program for Inverting Noisy Linear Algebraic and Integral Equations. *Comput. Phys. Commun*. **1982**, *27*, 229–242. DOI:10.1016/0010-4655(82)90174-6

[22] Scotti, A.; Liu, W.; Hyatt, J. S.; Herman, E. S.; Choi, H. S.; Kim, J. W.; Lyon, L. A.; Gasser, U.; Fernandez-Nieves, A. The CONTIN Algorithm and Its Application to Determine the Size Distribution of Microgel Suspensions. *J. Chem. Phys*. **2015**, *142*, 234905. DOI:10.1063/1.4921686

[23] Marino, I.-G. Regularized Inverse Laplace Transform (RILT) – MatLab Script. https://se.mathworks.com/matlabcentral/fileexchange/6523-rilt (accessed July 25, **2018**).

[24] Jonasson, J. K.; Lorén, N.; Olofsson, P.; Nydén, M.; Rudemo, M. A Pixel-Based Likelihood Framework for Analysis of Fluorescence Recovery After Photobleaching Data. *J. Microsc*. **2008**, *232*, 260–269. DOI:10.1111/j.1365-2818.2008.02097.x

[25] Van Blaaderen, A.; Vrij, A. Synthesis and Characterization of Colloidal Dispersions of Fluorescent, Monodisperse Silica Spheres. *Langmuir*. **1992**, *8*, 2921–2931. DOI:10.1021/la00048a013

[26] Wang, X.-D.; Shen, Z.-X.; Sang, T.; Cheng, X.-B.; Li, M.-F.; Chen, L.-Y.; Wang, Z.-S. Preparation of Spherical Silica Particles by Stöber Process with High Concentration of Tetra-Ethyl-Orthosilicate. *J. Colloid Interface Sci*. **2010**, *341*, 23–29. DOI:10.1016/j.jcis.2009.09.018

[27] Ow, H.; Larson, D. R.; Srivastava, M.; Baird, B. A.; Webb, W. W.; Wiesner, U. Bright and Stable Core – Shell Fluorescent Silica Nanoparticles. *Nano Lett*. **2005**, *5*, 113–117. DOI:10.1021/nl0482478

[28] Tansub, W.; Tuitemwong, K.; Limsuwan, P.; Theparoonrat, S.; Tuitemwong, P. Synthesis of Antibodies-Conjugated Fluorescent Dye-Doped Silica Nanoparticles for a Rapid Single Step Detection of Campylobacter jejuni in Live Poultry. *J. Nanomater*. **2012**, *2012*, 7.

[29] Santra, S.; Wang, K.; Tapec, R.; Tan, W. Development of Novel Dye-Doped Silica Nanoparticles for Biomarker Application. *J. Biomed. Opt*. **2001**, *6*, 160–166. DOI:10.1117/1.1353590

[30] Wang, L.; Wang, K.; Santra, S.; Zhao, X.; Hilliard, L. R.; Smith, J. E.; Wu, Y.; Tan, W. Watching Silica Nanoparticles Glow in the Biological World. *Anal. Chem*. **2006**, *78*, 646–654. DOI:10.1021/ac0693619

[31] van Blaaderen, A.; Vrij, A. Synthesis and Characterization of Monodisperse Colloidal Organo-Silica Spheres. *J. Colloid Interface Sci*. **1993**, *156*, 1–18. DOI:10.1006/jcis.1993.1073

[32] Stejskal, E. O.; Tanner, J. E. Spin Diffusion Measurements: Spin Echoes in the Presence of a Time-Dependent Field Gradient. *J. Chem. Phys*. **1965**, *42*, 288–292. DOI:10.1063/1.1695690

[33] Lipani, E.; Laurent, S.; Surin, M.; Vander Elst, L.; Leclère, P.; Muller, R. N. High-Relaxivity and Luminescent Silica Nanoparticles as Multimodal Agents for Molecular Imaging. *Langmuir*. **2013**, *29*, 3419–3427. DOI:10.1021/la304689d

[34] Santra, S.; Bagwe, R. P.; Dutta, D.; Stanley, J. T.; Walter, G. A.; Tan, W.; Moudgil, B. M.; Mericle, R. A. Synthesis and Characterization of Fluorescent, Radio-Opaque, and Paramagnetic Silica Nanoparticles for Multimodal Bioimaging Applications. *Adv. Mater*. **2005**, *17*, 2165–2169. DOI:10.1002/adma.200500018

[35] Kircher, M. F.; Mahmood, U.; King, R. S.; Weissleder, R.; Josephson, L. A Multimodal Nanoparticle for Preoperative Magnetic Resonance Imaging and Intraoperative Optical Brain Tumor Delineation. *Cancer Res*. **2003**, *63*, 8122–8125. http://cancerres.aacrjournals.org/content/63/23/8122.abstract.

[36] Morag, J.; Dishon, M.; Sivan, U. The Governing Role of Surface Hydration in Ion Specific Adsorption to Silica: An AFM-Based Account of the Hofmeister Universality and Its Reversal. *Langmuir*. **2013**, *29*, 6317–6322. DOI:10.1021/la400507n